Scaling Laws in the Transient Dynamics of Firefly-like Oscillators

2011 J. Phys.: Conf. Ser. 285 012026

(http://iopscience.iop.org/1742-6596/285/1/012026)

Journal of Physics: Conference Series **285** (2011) 012026 doi:10.1088/1742-6596/285/1/012026

SCALING LAWS IN THE TRANSIENT DYNAMICS OF FIREFLY-LIKE OSCILLATORS

N Rubido[1], C Cabeza[1], G. M. Ramírez Ávila[2,3] and A. Martí[1]

[1] Iguá 4225, Instituto de Física, Facultad de Ciencias, Montevideo, Uruguay.
[2] Institut für Physik, Humboldt Universität zu Berlin, Germany.
[3] Instituto de Investigaciones Físicas, Universidad de San Andrés, La Paz, Bolivia.

E-mail: nrubido@fisica.edu.uy

Abstract. Fireflies constitute a paradigm of pulse-coupled oscillators. In order to tackle the problems related to synchronisation transients of pulse-coupled oscillators, a Light-Controlled Oscillator (LCO) model is presented. A single LCO constitutes a one-dimensional relaxation oscillator described by two distinct time-scales meant to mimic fireflies in the sense that: it is capable of emitting light in a pulse-like fashion and detect the emitted by others in order to adjust its oscillation. We present dynamical results for two interacting LCOs in the torus for all possible coupling configurations. Transient times to the synchronous limit cycle are obtained experimentally and numerically as a function of initial conditions and coupling strengths. Scaling laws are found based on dimensional analysis and critical exponents calculated, thus, global dynamic is restricted. Furthermore, an analytical orthogonal transformation that allows to calculate Floquet multipliers directly from the time series is presented. As a consequence, local dynamics is also fully characterized. This transformation can be easily extended to a system with an arbitrary number of interacting LCOs.

1. Introduction

Pulse coupling is extensively common in Biology —the chirp of crickets, pacemaker cells firing and fireflies flashing, among many—. The study of how pulse-coupled oscillators achieve synchrony is important due to experimental observations of synchronous neural firing patterns of various animal species [1, 2]. However, the scope of synchronous behaviours runs far beyond neural dynamics [3, 4]. Synchronisation exhibits itself in physical [5], chemical [6], biological [7] and electronic [8] systems. Furthermore, phenomena involving synchronisation in complex networks [9, 10], chaotic systems [11] or time-delayed systems [12], have been intensively studied in recent years.

While experimental works dealing with these problems are usually based in complex models, transient times are only elucidated for simpler models in some configurations of phase locked loops [13] and Light-Controlled Oscillators (LCOs) [14, 15, 16, 17]. These oscillators constitute simple electronic devices that allow to study synchronisation dynamics in a simple way. From a theoretical point of view, synchronisation can be characterized studying transient times towards phase-locking states. In the vicinity of these state, transient regimes are equivalent to the study of reaching a limit cycle. Nevertheless, despite huge efforts, a general theoretical framework for global dynamics is still missing.

In this sense, we present a dimensional analysis that allows to calculate scaling laws for two coupled oscillators that restrict the global dynamics transients. In particular, the technique is exhibited for LCOs and compared with results from the well-known Kuramoto oscillators. On the other hand, a general orthogonal transformation deduced from the model that allows to calculate the Floquet eigenvector directions directly from the time series is presented. Using this transformation, the limit cycle multipliers for the torus local dynamics of coupled LCOs are calculated in the two possible configurations. Furthermore, an analytical extension of these transformations to higher dimensions is direct.

This paper is organized as follows. In Sec. 2, the LCO experimental set-up and analytical model is presented. In Sec. 3 we explain the phase variables and dynamical quantities relevant for the representation of the evolution of two coupled oscillators in the toroidal state space. Experimental and numerical results for transients behaviours are shown in Sec. 4. Finally, conclusions and perspectives are presented in Sec. 5.

2. Light-controlled oscillators (LCOs)

2.1. Experimental set-up

The LCOs presented here constitute one dimensional dynamical systems that oscillate in a piecewise analytic form with two characteristic time-scales: a slow charging stage and a fast discharge. IR light is emitted in a pulse-like fashion during discharge modifying the receiver's stage. Experimentally, each LCO is composed of an LM555 chip operating in an astable oscillating mode and a dual RC circuit [16, 17] with a common capacitor. The chip acts as a logical gate between these two circuits by establishing well-defined thresholds for the capacitor voltage: $2V_{cc}/3$ and $V_{cc}/3$, being V_{cc} the source voltage. As a consequence, one RC-circuit defines the charging stage as long as the upper threshold is not achieved. Whenever the upper threshold is reached, the chip switches to the other RC-circuit, generating the discharging stage until the lower threshold is attained. During the discharge, the system emits an Infra-Red (IR) light pulse by means of LEDs connected in series with the resistors.

The associated charging and discharging times may be adjusted by modifying the resistors R_λ and R_γ connected in series with the LEDs. The duration of these stages are set in the order of milliseconds for experimental practicality. The period of each oscillator is determined by the sum of these time intervals. IR emissions can be detected due to the inclusion of photo-diodes set in parallel with the RC circuits. Consequently, pulse detection modifies at any instant the charge in the capacitor, increasing its voltage in either stage. Thus, shortening the charging stage and/or lengthening the discharge.

The time-scale parameters of LCOs are chosen in a way that the resulting oscillating pattern resembles an integrate-and-fire model (firing interval corresponds to $\sim 1\%$ of the total period), as this oscillating form results in smaller transients. Coupling strengths can be modified by two means: varying the distance between oscillators or by forcing smaller emissions due to the addition of an extra resistor connected in series with the LEDs. On the other hand, different coupling configurations can be attained if photo-sensors are masked differentially. An uncoupled LCO is named as, *in dark*. No time delays in the couplings are considered, in view of the characteristics of the light pulses.

The experimental measurements have been carried out using a data acquisition card (NI-DAQ) that allowed us to obtain all the underlying dynamics of the system with a 20kHz sampling rate. Each LCO has its own source voltage, all set approximately equal to $V_{cc} = 9$V. Therefore, different initial conditions are generated by switching on the sources in a differential way. However, this method results in a random initial charging state, thus, many measurements are done in order to have a uniform distribution of initial conditions throughout the voltage domain $[V_{cc}/3,\ 2V_{cc}/3]$.

2.2. Dynamical model

From a dynamical point of view, an LCO presents a one-dimensional flow, periodic and continuous, nevertheless, piecewise analytic. Charging and discharging time-scales are related to the RC characteristics. For the uncoupled dynamics, these scales can be expressed as a function of the circuit parameters by:

$$\begin{cases} T_\lambda^0 = \frac{\log(2)}{\lambda} = \log(2)\ (R_\lambda + R_\gamma)\ C\,, \\ T_\gamma^0 = \frac{\log(2)}{\gamma} = \log(2)\, R_\gamma\, C\,, \end{cases} \tag{1}$$

where λ (γ) is the inverse charging (discharging) characteristic time-scale, and the superscript ^{0} is used to denote the *in dark* value. Figure 1 shows a typical *in dark* LCO evolution.

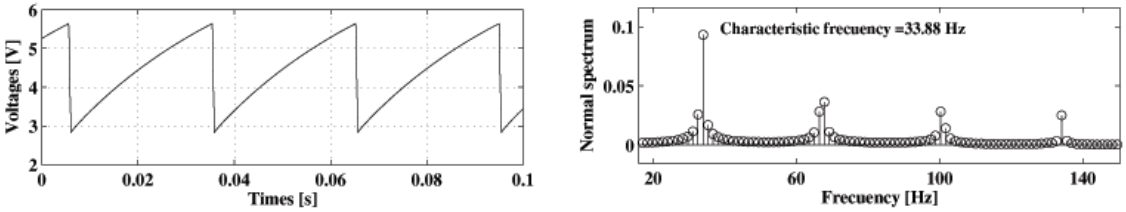

Figure 1. Time window for the *in dark* voltage evolution of an LCO (left panel) and frequency spectrum (right panel) for typical parameter values.

Based on the nature of the electronic devices that constitute an LCO and their experimental behaviour, the system of LCOs interacting is described by the following set of piecewise linear differential equations:

$$\dot{V}_i(t) = \lambda_i\,[V_{cc} - V_i(t)]\,\epsilon_i(t) - \gamma_i V_i(t)\,[1-\epsilon_i(t)] + \sum_{j=1,\,j\neq i}^{N} \beta_{ij}\,[1-\epsilon_j(t)],\ i = 1,\ldots,N, \tag{2}$$

being $V_i(t)$ the instantaneous voltage of the i-th oscillator of the set of N coupled LCOs and ϵ_i a discrete variable that can take the values 0 (discharge) or 1 (charge) according to the capacitor stage. This variable is created for each LCO in order to represent the change of stage and to simplify the notation of the set of differential equations of the voltage.

Equation (2) shows that the coupling is caused by the addition of a constant value: $\sum_k \beta_{ik}$, where k is an index that takes into account only the LCOs from the set that are discharging at that particular instant. We consider that all elements of the coupling matrix are non-negative and that there is no feedback, meaning that all diagonal elements are null. In particular, for two coupled LCOs, the coupling matrix can be characterized by two distinct forms: the master-slave (MS), where there is only one interaction in play, thus, one LCO acts as an external forcing to the other; and mutual-interaction (MI), where both LCOs interact. This coupling forms constitute the configurations dealt within this paper.

3. Evolution in the torus

LCOs constitute one-dimensional oscillators, thus, a pair of interacting LCOs can be described by phase angle variables that evolve in a toroidal states space. These phase variables are directly linked to the voltage evolution.

3.1. Voltage phase variables

The ith-oscillator of the set described by Eq.(2) can be described at all times by a pair of variables (V_i, ϵ_i), though, the only dinamical variable relevant of these is the voltage. The proof lies in the construction of the state space of the corresponding oscillator and its phase variable. While $\epsilon = 1$ the voltage increases monotonically, whereas, when $\epsilon = 0$ it decreases.Thus, a phase variable can be constructed directly from the voltage evolution taking these two stages into account by the use of a simple symmetry operation.

According to the pair of variables (voltage and stage), the evolution of a single LCO is always restricted to a state space composed of two intervals of equal length ($[V_{cc}/3,\, 2V_{cc}/3]$) that are connected in a discontinuous fashion by the discrete stage variable (ϵ). Coupling affects the time that the LCO spends in each stage. If these discontinuities are removed by connecting the two capacitor stages in a convenient way, the state space could be transformed into a circle. Assuming monotonicity, a phase variable can be constructed reflecting the discharging stage around its mean value and making a proper voltage translation. This transformation corresponds to passing from the initial oscillating state:

$$[V_{cc}/3,\, 2V_{cc}/3]\,,\ \epsilon = 1 \rightarrow [2V_{cc}/3,\, V_{cc}/3]\,,\ \epsilon = 0, \rightarrow [V_{cc}/3,\, 2V_{cc}/3]\,,\ \epsilon = 1 \rightarrow \cdots,$$

to a situation where the interval of voltages expands to $[V_{cc}/3,\, V_{cc}]$ in the following manner,

$$[V_{cc}/3,\, 2V_{cc}/3]\,,\ \epsilon = 1 \rightarrow [V_{cc}/3,\, 2V_{cc}/3] + V_{cc}/3,\ \epsilon = 0 \rightarrow [V_{cc}/3,\, 2V_{cc}/3]\,,\ \epsilon = 1 \rightarrow \cdots.$$

Therefore, a phase variable can be created directly from this evolution due to the fact that voltage now increases monotonically along a simple period for any coupling situation. Once the lower voltage threshold of the discharging situation is reached (which after the symmetry operations corresponds to a voltage of V_{cc}), then the oscillation retraces its evolution and the voltage is set to $V_{cc}/3$ in a charging stage ($\epsilon = 1$). As a consequence, a new voltage variable that increases monotonically can be expressed as a function of this new oscillating form, simply by adding V_{cc} after a period has passed.

Naming this new voltage variable for all LCOs as $\tilde{V}_i$, the phase angle variable is defined as:

$$\phi_i\,(t) = \pi\,\frac{\tilde{V}_i\,(t) - V_{cc}/3}{V_{cc}/3}\,,\ \ \forall\, i = 1,\, \ldots,\, N\,. \tag{3}$$

For instance, starting from $V(0) = V_{cc}/3$, when the LCO reaches for the first time the upper threshold ($V\,(T_\lambda) = VV\,(T_\lambda) = 2V_{cc}/3$) the phase angle is π, whereas when it reaches the lower threshold ($V(T_\lambda + T_\gamma) = V_{cc}/3$ corresponding to $\tilde{V}(T) = V_{cc}$), the phase increases to take the value 2π.

3.2. State space

By means of the phase angle variables, a pair of LCOs can be described in a toroidal state space with a continuous evolution depicted in Fig. 2. It has been shown [18] analytically that the system exhibits two fixed points in the return map (one stable and the other unstable) for a wide range of frequency detuning between oscillators and coupling strengths. Thus, coupled dynamics tends to create two limit cycles, one attractive and other repelling.

The standard variance of two voltage time series is defined as the time average ($\langle\cdot\rangle$) of the voltage difference by:

$$\sigma^2 = \frac{1}{2}\left\langle\left(\frac{V_1 - V_2}{2}\right)^2\right\rangle. \tag{4}$$

Transients are then investigated using a Poincaré section of the flow as well as taking the standard variance σ^2 of the whole time series. The first method allows to calculate

synchronisation times by adding the return times that the system needs to achieve the fixed point of the return map. On the other hand, σ^2 is generally used to measure the synchronicity of a system after transients have died out. If synchronised, $\sigma^2 \to 0$, nevertheless, it does not need to withdraw any portion of the time series if transient calculations are being made. In this cases, the value of σ^2 increases if the transient is longer, thus, σ^2 will measure the initial condition dependence of the system.

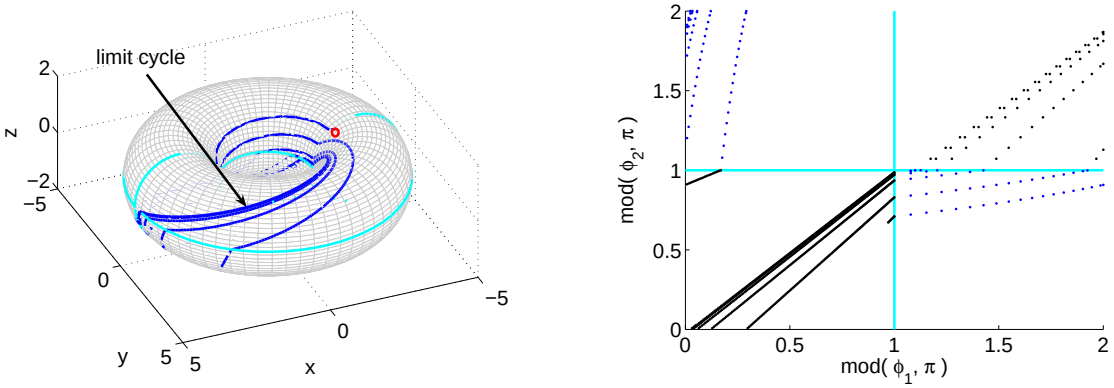

Figure 2. Numeric transient dynamics for two coupled LCOs in a MS configuration with $\beta = 200\ V/s$ and an initial voltage difference of $\Delta V(0) = 0.3\ V$ with both LCOs charging. In the right panel, the toroidal state space is represented. The flow is presented with blue lines, the initial state with a red circle and cyan lines represent a guide for the eye in order to recognize the four possible voltage stages. The same system is exposed in the right panel, where charging-charging stages and discharging-discharging stages are represented with black dots and mixed stages with blue dots (sampling rate: $10\,kHz$). The slow and fast evolution characteristics of each region are directly unveiled in this representation.

These methods are used to show that the global dynamic behaviour is restricted in a somehow universal fashion, leading to scaling laws of the system that make transient paths independent of coupling strengths (β) with the aid of proper dimensionless variables.

As the right panel in Fig. 2 shows, the attractive limit cycle corresponds to the diagonal of T^2. Thus, a simple orthogonal transformation of the state space would inevitably lead to create the Floquet eigenvectors that allow to calculate the local dynamic multipliers.

The coordinate transformation needed is a counter-clockwise rotation of 45° of the T^2 covering state space variables (right panel in Fig. 2) around the origin. This fact implies that the new coordinate system is:

$$\tilde{\phi}_1 = \frac{\phi_2 + \phi_1}{\sqrt{2}}\,, \quad \tilde{\phi}_2 = \frac{\phi_2 - \phi_1}{\sqrt{2}}\,, \tag{5}$$

where the $\tilde{\phi}_1$ new coordinate corresponds to the diagonal, thus a null multiplier is expected, and $\tilde{\phi}_2$ is the normal limit cycle coordinate. The same transformation can be applied to the voltage time series and the results are identical.

4. Results

4.1. Local dynamics

Equation (5) is an orthogonal transformation that can be easily generalized to higher dimension systems, due to the fact that the *quid* of the question lies in the fact that the synchronisation limit cycle of N coupled LCOs always lies in the covering state space diagonal. Thus, for higher dimensions, a composition of these transformations can generate all Floquet eigenvectors [19].

Therefore, a direct analysis from the transformed voltage time series can be done in order to calculate Floquet multipliers (see the right panel in Fig. 3).

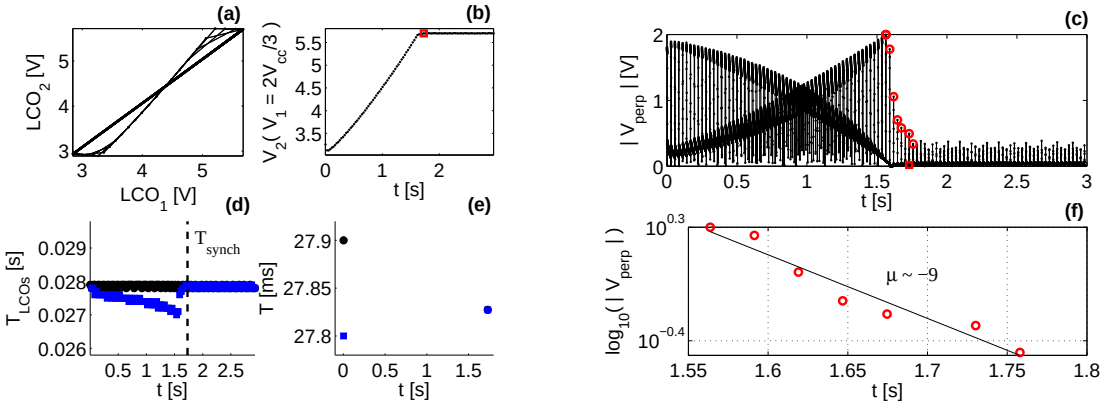

Figure 3. Experimental time series analysis of two coupled LCOs in MS configuration. In panel **(a)**, the Lissajous figure of the synchronised state is shown. In panel **(b)**, the Poincaré return map evolution with a red square that corresponds to the synchronisation time is plotted. The transformed voltage series for the cycle normal coordinate corresponds to panel **(c)**. Red circles correspond to the exponential decay in amplitude of the coordinate, and are represented in logarithmic fashion in panel **(f)**. Panel **(d)** displays the period evolution of the two coupled LCOs, and panel **(e)** the corresponding initial and final (synchronised) values.

Experimental results show that the Floquet multipliers μ for both directions in MS configuration and all initial conditions in average are:

$$\begin{cases} \bar{\mu}_2 = -10.45 \pm 0.29 \\ \bar{\mu}_1 = 0.012 \pm 0.02 \end{cases}, \tag{6}$$

where $\bar{\mu}_2$ ($\bar{\mu}_1$) corresponds to the normal (parallel) direction with respect to the limit cycle averaged over all initial conditions used. This shows that Floquet exponents should be independent from initial conditions as expected. Nevertheless, it is also found that exponents for two coupled LCOs are independent of the coupling strength and only depend on the coupling configuration, in other words, if they are coupled via an MS or MI configuration.

In order to improve the calculations of these exponents and reduce the noise coming from the experimental time series (caused by minor noise fluctuations of the source voltage), new calculations are being done over the time series. As the T^2 evolution in the right panel of Fig. 2 shows, the flow reaches the diagonal only on the $(\epsilon_1, \epsilon_2) = (1, 1)$ region (lower left section). Whereas in the $(0, 0)$ (upper right section) is slightly translated. This is explained by analysing the return maps, where the fixed point is not located exactly in a corner [18]. Therefore, calculations of Floquet exponents introduce a systematic error that can be dismissed if the charging part of the time series is taken into account. This problem is increased when Floquet exponents are calculated for MI configuration, thus, μ_2 results in greater dispersion from $\bar{\mu}_2 \sim -7$.

4.2. Experimental and numerical synchronisation times

The experimental results obtained for MS and MI configurations for the synchronisation times as a function of initial coupling voltages are shown in Fig. 4. The initial time is taken to be the first time one of the two LCOs reaches the upper threshold for the first time due to the fact that former states can be treated as uncoupled dynamics. Thus, the name initial coupling voltage.

The LCO_1 and LCO_2 period *in dark* for the MS configuration are $T_1^{dark} = 28.6$ ms, $T_2^{dark} = 28.4$ ms; and for the MI configuration are $T_1^{dark} = 24.7$ ms, $T_2^{dark} = 24.3$ ms. Different coupling strengths are achieved by placing LCOs at different distances from each other. Distances used are: $d_1 = 5$ cm, $d_2 = 10$ cm, $d_3 = 15$ cm, $d_4 = 20$ cm and $d_5 = 25$ cm. Then, the connectivity matrix elements are calculated directly from the resulting time series by comparison with the solutions of the Eq.(2) for these parameters.

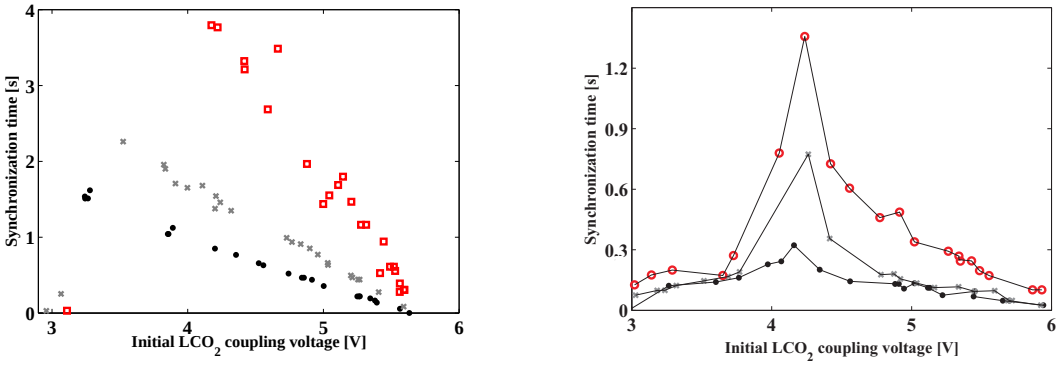

Figure 4. Synchronisation times as a function of the initial coupling voltage of LCO_2 in MS (left figure) and MI (right figure) configuration (LCO_1 initial voltage corresponds to the first time that it starts to discharge, meaning that $V_1(0) = 2V_{cc}/3$). Red circles (right panel) correspond to a distance d_4, squares (left panel) to d_3, grey crosses to d_2 and black points to d_1. On the right hand side a thin black line that conects the data is showed as a guide for the eye. LCO_1 is taken as the leader (or master) LCO.

Experimental synchronisation times for both configurations are resolved from the Poincaré section corresponding to registering voltages every time LCO_1 reaches the upper threshold (starts to discharge). As can be seen from these figures, there is a single initial condition value for LCO_2 voltage that gives a nearly asymptotic behaviour for all configuration schemes. This value reveals the repeling limit cycle that would correspond to a null synchronisation time. Experimental results cannot achieve this state due to the action of electronic noise, that presents itself as a kind of symmetry breaker. Moreover, these figures demonstrate that all initial conditions are attracted to the synchronisation manifold as is expected.

In an analogous fashion, numerical synchronisation times are resolved, both, by the Poincaré section and by Eq.(4). Figure 5 exhibits the resultant curves as a function of initial conditions for the MI configuration of coupled LCOs and Kuramoto oscillators. The Kuramoto model is represented by:

$$\begin{cases} \dot{\theta}_1 = \omega_1 + K \sin(\theta_1 - \theta_2) , \\ \dot{\theta}_2 = \omega_2 + K \sin(\theta_2 - \theta_1) , \end{cases} \tag{7}$$

where K is the coupling strength (it is comparable only with β/V_{cc}). Time-scale parameters for both systems are set in order to have identical individuals oscillating at a $\omega = 30$ rad/s frequency. The Kuramoto model is solved by means of a fourth order Runge-Kutta schemes, whilst LCOs are solved by using piecewise analytic solutions numerically implemented as in previous works [18].

As can be seen from these figures, transients behave in a self-similar way. Therefore, scaling laws should be possible to find in order to achieve a universal form. In Sec. 4.3 we present a method that uses the single initial condition that correspond to the nearest registered value to the repelling limit cycle to scale all quantities. The analysis made is based on dimensional analysis.

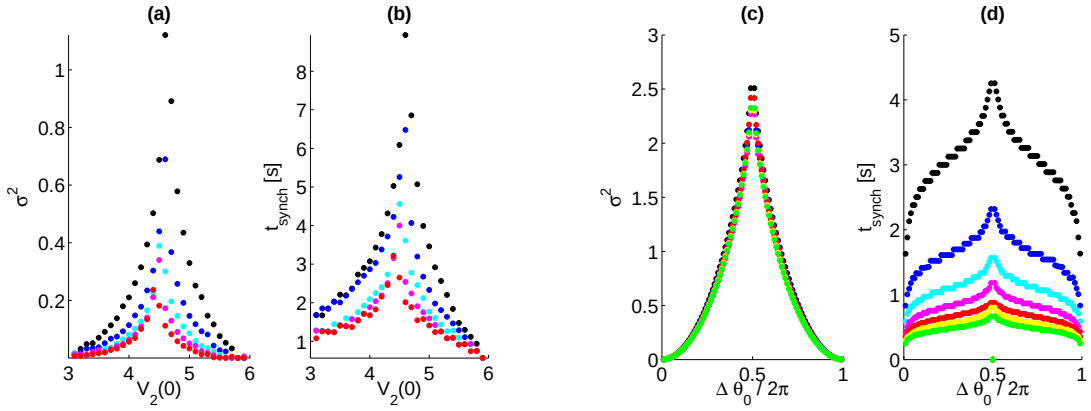

Figure 5. Panels **(a)** and **(b)** show the numerically simulated transients for two coupled identical LCOs in MI configuration. Voltage initial conditions can also be represented as phase angular variables using Eq.(3). Panels **(c)** and **(d)** exhibit the same dynamic for two coupled Kuramoto oscillators. For LCOs, coupling strengths correspond to $\beta = 100$ (black dots), 150 (blue), 200 (cyan), 250 (magenta) and 300 V/s (red). On the other hand, $K \simeq 1.21$ (black dots), 2.32 (blue), 3.43 (cyan), 4.54 (magenta) and 6.76 rad/s (red).

4.3. Global dynamics

As can be seen from both configurations plotted in Fig. 4, synchronisation times exhibit self-similar forms as functions of initial conditions for all coupling strengths. Thus, scaling laws are sought and critical exponents calculated. In particular, we consider that a MS configuration is achieved for a connectivity matrix given as $\beta_{12} = 0$ and $\beta_{21} = \beta$, while a MI configuration is formed by having $\beta_{12} = \beta_{21} = \beta$.

In order to achieve the scaling laws for these configurations we have to consider a dimensionless version of the model given in Eq.(2). Therefore, voltage signals are normalized using the source voltage ($V_n = V/V_{cc}$), times variables are made dimensionless by using LCO_1 *in dark* period ($t_n = t/T_1^0$), and as a result, β is changed to $\tilde{\beta} = T_1^0\beta/V_{cc}$. Then, the Pi theorem [20] assures that the relevant dimensionless parameters needed to describe the particular dynamic transient are: the initial voltage difference (in particular, the LCO_2 voltage, V_n^{init}), the synchronisation time (t_n^{synch}) and the coupling strength $\tilde{\beta}$, which obey a certain functional relation expressed as:

$$t_n^{synch} = f\left(V_n^{init}, \tilde{\beta}\right) . \tag{8}$$

The self-similar behaviour found in both configurations for the experimental and numerical solutions of Eq.(2), allows to define two characteristic dynamical scales: the dimensionless maximum time, namely $t^* := \max\left(t_n^{synch}\right)$, and the corresponding dimensionless initial voltage, namely $V^* := V_n^{init}\left(t^*, \tilde{\beta}\right)$. These scales represent the nearest location to the repelling limit cycle that in T^2 the system can achieve. They are used to achieve the collapse of the transient curves and to find the scaling exponents that relates t^* with the ratio $V^*/\tilde{\beta}$. The exponents found correspond to the following linear relation

$$\log\left(t^*\right) = \alpha \log\left(\frac{V^*}{\tilde{\beta}}\right) + \kappa. \tag{9}$$

The exponents found for these linear relation in the configurations analysed are:

$$\left\{ \begin{array}{ll} \alpha_{exp}^{MS} = 0.71\,, & \kappa_{exp}^{MS} = 1.76 \\ \alpha_{num}^{MS} = 1.04\,, & \kappa_{num}^{MS} = 1.96 \end{array} \right. , \quad \left\{ \begin{array}{ll} \alpha_{exp}^{MI} = 0.74\,, & \kappa_{exp}^{MI} = 2.00 \\ \alpha_{num}^{MI} = 0.88\,, & \kappa_{num}^{MI} = 2.06 \end{array} \right. , \tag{10}$$

giving a relative difference between numeric and experimental values of

$$\begin{cases} \Delta\alpha/\alpha_{num} = 0.32 \\ \Delta\kappa/\kappa_{num} = 0.10 \end{cases}, \quad \begin{cases} \Delta\alpha/\alpha_{num} = 0.16 \\ \Delta\kappa/\kappa_{num} = 0.03 \end{cases}.$$

Once exponents and scaling laws are calculated, collapse curves are obtained by plotting

$$\frac{t_n^{synch}}{t^*} = \frac{f\left(V_n^{init}/V^*, \tilde{\beta}\right)}{10^{\kappa}\left(\frac{V^*}{\tilde{\beta}}\right)^{\alpha}} = g\left(\frac{V_n^{init}}{V^*}\right). \tag{11}$$

Results of this universal behaviour are presented in Fig. 6. It can be seen directly from the graphics, that numerical simulations reinforce the universality expectations of the transients as the collapsed curves exhibit great agreement.

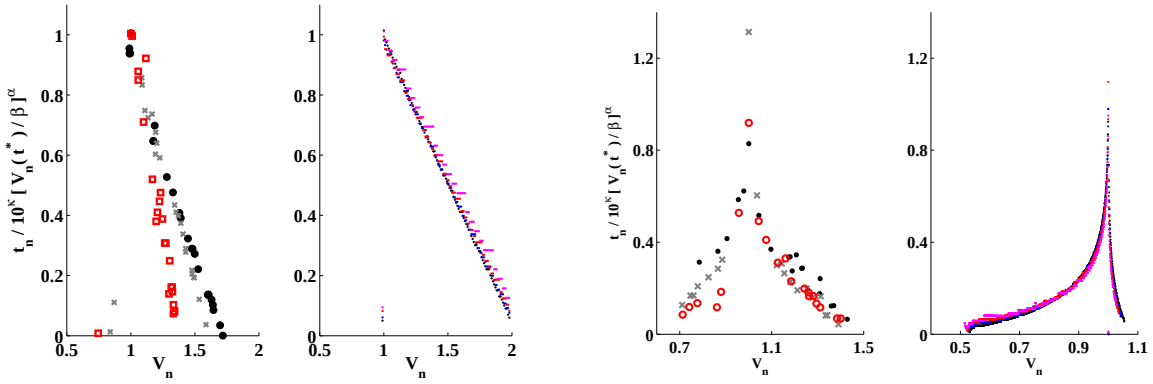

Figure 6. Synchronisation times collapsed as a function of the dimensionless LCO_2 initial conditions for the MS (two left panels) and MI (two right panels) configuration. For both configurations, the experimental data are plotted on the left and the numerical simulations on the right. Numerical simulations (dots) correspond to different coupling strengths: $\beta = 250$ (black), 200 (blue), 150 (red) and 50 (magenta) V/s and time-scale parameters given in Sec. 4.2.

5. Conclusions

The design of LCOs allowed us to modify on the spot their intrinsic period and pulse-like IR light emissions, enabling quantitative measurement of phase differences and period variations with fine precision, and produce electronically and physically different coupling strengths. This electronic set-up allowed us to obtain synchronisation times as well as stable states.

The evolution of the system in state space was used to construct phase variables and retrieve local dynamic behaviours by means of Floquet multipliers. The orthogonal transformation method that we present can be generalized to higher dimensions. Thus, systems with many interacting LCOs can also have their local dynamics quantified. Results in this matter corroborate that multipliers are independent of initial conditions. Nevertheless, for both configurations, exponents also seem to be independent of the coupling strength used. Current work is being done in order to improve the exponents calculations. The new method restricts the transformation to the charging-charging region of T^2.

The search for scaling exponents is done in order to analyse the transients global dynamics independently of the coupling strength, meaning that we can disregard the physical coupling

magnitude used when studying the synchronisation times for coupled LCOs in MS and MI configurations. Also, these exponents constitute a classification of the LCOs transients within a certain universality class of relaxation oscillators yet to be found, regardless of their particular dynamics. With this spirit is that results from Kuramoto model are shown. Nevertheless, the self-similar behaviour that this system also shows when the oscillators are identical does not accept the similar scales than LCOs do in order to create the collapsed curves. This is due to the fact that the nearest initial condition to the repelling limit cycle does not change location if coupling strength is varied when Kuramoto model is investigated. However, recent results with non-identical Kuramoto oscillators retrieve the LCOs scale choice.

Scaling results for LCOs were contrasted with numerical ones showing good agreement in MI configuration. MS mismatch can be explained by observing Fig. 4, where experimental synchronisation times for smaller coupling strengths were not recorded for an interval around the asymptotic state initial condition. Thus, the maximum synchronisation time registered is not a reliable quantity. This recording problem is inherent in our initial condition experimental extracting method, due to the fact that initial conditions are randomly generated, and in practice the system seems to avoid these asymptotic state. Currently, these problems are addressed as part of future works.

Finally, the dimensional analysis that helps to introduce the scaling laws shows promising results and constitute a great encouragement for further studies and generalizations of this model. Paths to be followed, can be different characteristic time-scale ratios or LCOs coupled networks, where currently achieved simulations exhibit self-similar transient behaviours for three coupled LCOs in various configuration schemes. Results in these lines would show the versatility and experimental value of the model.

6. Acknowledgements

We acknowledge financial support from PEDECIBA, CSIC (U. de la República, Uruguay) and ANII (Uruguay).

References

[1] Lehnertz K, *et al* 2009, *J. Neuroscience Methods*, **183**, 42-48.
[2] Sandra R.F.S.M. Gois and Savi M A 2009, *Chaos, Solit. and Fract.*, **41**, 2553-2565.
[3] Hodgkin A L and Huxley A F 1952, *J. Physiol.*, **117**, 500-544.
[4] Fitzhugh R 1961, *Biophys. J.*, **1**, 445466.
[5] Argonov V Yu and Prants S V 2005, *Phys. Rev. A*, **71**, 053408-11.
[6] Fukuda H, Morimura H and Kai S 2005, *Physica D*, **205**, 80.
[7] Glass L 2001, *Nature* (London), **410**, 277.
[8] Pisarchik P A, Jaimes-Reátegui R and García-López J H 2008, *Int. J. Bif. Chaos*, **18**, 1801.
[9] Timme M, Wolf F and Geisel T 2002, *Phys. Rev. Lett.*, **89**, 258701.
[10] Zumdieck A, Timme M, Geisel T and Wolf F 2004, *Phys. Rev. Lett.* **93**, 244103.
[11] Mahmoud G M, Aly S A and Farghaly A A 2007, *Chaos, Sol. & Fract.*, **33**, 178-187.
[12] Masoller C and Martí A C 2005, *Phys. Rev. Lett.*, **94**, 134102.
[13] Goldsztein G and Strogatz S H 1995, *Int. J. Bif. Chaos.*, **5**, 983.
[14] Mirollo R E and Strogatz S H 1990, *SIAM J. App. Math.*, **50**, 1645.
[15] Bottani S 1995, *Phys. Rev. Lett.*, **74**, 4189.
[16] Ramírez Ávila G M, Guisset J L and Deneubourg J L 2003, *Physica D*, **182**, 254.
[17] Rubido N, Cabeza C, Martí A C and Ramírez Ávila G M 2009, *Phil. Trans. Royal Soc. A*, **367**, 3267-3280.
[18] Rubido N, Cabeza C, Kahan S, Ramírez Ávila G M and Martí A C 2010, *Eur. Phys. J. D*, DOI 10.1140/epjd/e2010-00215-4.
[19] Guckenheimer J and Holmes P, *Nonlinear Oscillations, Dynamical Dystems, and Bifurcations of Vector Fields* (Springer-Verlag, 1983).
[20] Buckingham E 1914, *Phys. Rev.*, **4**, 345376.